Original Article
pISSN 1738-2637 / eISSN 2288-2928
J Korean Soc Radiol 2017;77(5):286-297
https://doi.org/10.3348/jksr.2017.77.5.286

대한영상의학회지

Identifying CT-Based Risk Factors Associated with Synchronous Liver Metastases in Colorectal Cancer
다중검출 전산화단층촬영을 이용한 대장암 간전이의 위험인자 연구

Cho Rong Seo, MD, Seung Joon Choi, MD*, Hyung Sik Kim, MD
Department of Radiology, Gachon University Gil Medical Center, Incheon, Korea

Purpose: The aim of this study was to determine the radiologic risk factors of colorectal cancer (CRC) with synchronous liver metastases.
Materials and Methods: A total of 197 patients with CRC who had a visible tumor on contrast-enhanced abdominopelvic computed tomography and were treated between January 2012 and December 2012 were included. Longitudinal diameter, mural thickness, primary tumor attenuation, and other metastases were evaluated independently. Univariate analysis and multivariate logistic regression analysis were used to identify risk factors associated with the presence of liver metastases.
Results: Cases were divided into two groups based on the presence or absence of liver metastases (n = 56 and 141, respectively). Primary tumors with enhancement of ≥ 90 Hounsfield units (HU) were found to have a higher risk of liver metastases than those with enhancement of < 90 HU [odds ratio (OR): 2.619, p = 0.034]. The presence of pulmonary metastases was associated with a higher risk of liver metastases (OR: 14.218, p = 0.025). The presence of lymph node metastases (N2 vs. N0) and carcinoembryonic antigen (CEA) level independently predicted the presence of liver metastases (OR: 8.766, p < 0.001; OR: 1.012, p = 0.048).
Conclusion: The identified risk factors of synchronous liver metastases in CRC were tumor mural enhancement, pulmonary metastases, lymph node metastases, and CEA level.

Index terms
Colorectal Neoplasms
Liver Neoplasms
Tomography, X-Ray Computed

Received February 15, 2017
Revised April 14, 2017
Accepted June 22, 2017
***Corresponding author:** Seung Joon Choi, MD
Department of Radiology, Gachon University Gil Medical Center, 21 Namdong-daero 774beon-gil, Namdong-gu, Incheon 21565, Korea.
Tel. 82-32-460-3059 Fax. 82-32-460-3045
E-mail: sjchoi1118@gmail.com

INTRODUCTION

Colorectal cancer (CRC) is one of the most common cancers and the second leading cause of cancer-related death worldwide. At diagnosis, 14.5–25% of CRC patients have synchronous liver metastasis, and another 25–30% of CRC patients will develop liver metastasis during the next 2–3 years (1-4). The liver is the most common site of metastases, and liver metastasis is responsible for the death of at least two thirds of patients with a colorectal malignancy (5, 6). Early diagnosis of colorectal liver metastases (CLM) is important in terms of overall survival, and metastasis is the major cause of death in patients with CRC and its prevalence has been shown to depend on tumor stage (7). During the last few decades, resection of liver-limited CLM has been increasingly accepted by surgeons and oncologists, and improvements observed in outcome appear to be associated with increased use of hepatic resection or ablation therapy (8, 9). Some studies conducted in patients who have undergone complete surgical resection of liver metastases suggest that overall survival rates exceed 50% at 5 years and range from 17% to 25% at 10 years (10-12). Although neo-adjuvant chemotherapy has the potential to convert initially unresectable disease into resectable disease in some patients, the frequency of conversion and overall survival remain relatively low. It was reported that in patients with initially unresectable CLM, the 3-year overall survival rate was 30% after chemotherapy, and the median survival times were 24.4 and 25.8 months in cetuximab or bevacizumab combined with chemotherapy groups, respective-

ly (13, 14) .

Previous studies have reported that mesorectal vascular and fascia invasion by rectal magnetic resonance imaging (MRI) in rectal cancer patients independently predict early metastases (15, 16), and thus, it was suggested that liver MRI should be performed at diagnosis in high risk patients. Recently, a clinical trial (SERENADE) was initiated to determine the usefulness of DW-MRI for screening synchronous liver metastases in high risk primary CRC patients (17). However, in colon cancer, computed tomography (CT) continues to be used for risk analysis, because abdominal MRI for colon cancer is limited by respiration control and motion artifact. Furthermore, little information is available regarding the risk factors of liver metastasis in CRC patients as determined by CT. Accordingly, we undertook the present study to identify predictors of the presence of synchronous liver metastases in CRC.

MATERIALS AND METHODS

This retrospective study was approved by our Institutional Review Board, which waived the requirement for obtaining informed consent (GAIRB 2017-195).

Patient Population

We retrospectively reviewed our institutional electronic medical database of 364 patients with pathologically proven adenocarcinoma of the colon and rectum who were diagnosed between January 2012 and December 2012. One hundred sixty-seven patients were excluded for the following reasons: no visible measurable primary CRC on CT (n = 133); no preoperative CT scan (n = 3); refusal of further treatment at our institute (n = 14); and the presence of another primary cancer (n = 17). Finally, 197 patients were enrolled in this study (Fig. 1).

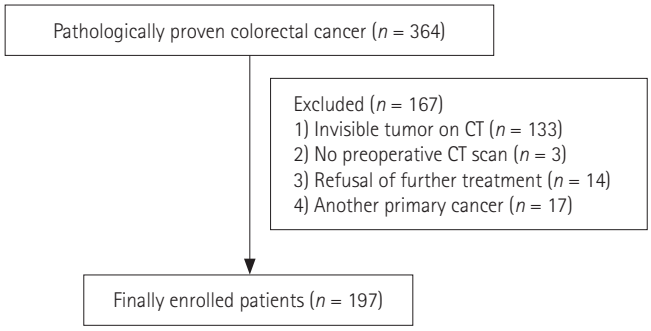

Fig. 1. Flow chart of patient enrollment.

CT Protocol

All patients underwent contrast-enhanced multi-detector CT including triple phase CT, double phase CT (arterial and portal venous phases), or single-phase CT (portal venous phase) with 16 detectors or 64 detectors (Somatom Sensation, Definition 64 and Somatom Definition Flash; Siemens Medical Solutions, Erlangen, Germany). Images of arterial and portal venous phases were obtained with a delay of 17–18 seconds and 50–51 seconds, respectively, after descending aorta attenuation reached 100 Hounsfield units (HU). Delayed scans were performed using a fixed delay of three minutes after contrast medium injection. Portal venous single phase imaging was performed one minute after descending aorta attenuation reached 50 HU. CT images were obtained during a breath-hold using the following parameters: 24-mm collimation; table feed, 24–36 mm/rotation; pitch, 1.0–1.5; 150–200 mAs; and 140 kVp. Images were reconstructed using 5-mm and 3-mm slice thicknesses in the transverse and coronal planes with no overlap. Nonionic contrast agent (Iohexol, Bonorex 300, Central Medical System, Seoul, Korea; Iopamidol, Pamiray, Dongkook Pharmaceutical, Seoul, Korea; Iopromide, Ultravist 300, Schering, Berlin, Germany) was injected at a dose of 2 mL/kg of body weight (to a maximum of 150 mL) via 18-gauge peripheral venous access at a flow rate of 4 mL/s using an automatic power injector (OptiVantage, Liebel-Flarsheim; Mallinckrodt, Neustadt, Germany).

MRI Protocol

MRI imaging was performed using a 1.5-T unit (Avanto; Siemens Medical Solutions) equipped with a body and spinal matrix coil. MRI images were acquired with use of the following parameters: a fat-suppressed, respiratory-triggered, T2-weighted turbo spin-echo sequence [repetition time (TR)/echo time (TE) of 3500–5000/70–85, echo train length of 10, 140° flip angle, matrix 202 × 320, 3-mm slice thickness], a breath-hold T2-weighted turbo spin-echo sequence (TR/TE of 2500–4500/103, 140° flip angle, matrix 202 × 320, 5-mm slice thickness), T2-weighted HASTE sequence (TR/TE of 400–500/100–150, 150° flip angle, matrix 166 × 256, 3-mm slice thickness), and a breath-hold T1-weighted fast low-angle shot sequence [TR 172, TE 2.46 (in-phase)/3.69 (out-of-phase)], 65° flip angle, matrix

208 × 256, signal average of one, two acquisitions, 5-mm slice thickness). Dynamic imaging was performed after an intravenous injection of contrast medium, 0.1 ml/kg of Gd-EOB-DTPA (Primovist, Bayer Schering Pharma, Berlin, Germany). The hepatic arterial, portal-venous, and transitional phase images were acquired at 40 s, 60 s, and 120 s, respectively, after commencing the Gd-EOB-DTPA injection. Contrast medium was injected using an automated injector at a rate of 2 mL/sec and the lines were flushed with 25 mL of saline solution after contrast injection.

Image Analysis

All primary tumors were clearly visualized on CT scans and were analyzed retrospectively using a Picture Archiving and Communication System. Images were independently evaluated on a workstation using a soft-tissue window setting by two radiologists (S.J.C with 7 years' experience in abdominal imaging and C.R.S with 4 years' radiology training) who were unaware of clinical information, laboratory findings, colonoscopy images, and surgical and pathologic reports. The following variables were included in the analysis on CT images: tumor location, longitudinal tumor length, tumor mural thickness, tumor attenuation [determined by placing a region of interest (ROI)], tumor shape, and pericolic fat infiltration.

Tumor locations were classified as right colon (cecum, ascending colon, hepatic flexure, and transverse colon), left colon (splenic flexure, descending and sigmoid colon), recto-sigmoid junction, and rectal ampulla. Longitudinal tumor diameter, mural thickness, and ROIs were measured on portal-venous phase CT scans. During each measurement session, tumor diameters and ROIs were measured independently by the two radiologists and mean values were recorded. Longitudinal tumor diameter was defined as the greatest tumor length along the longitudinal axis of the colon using both transverse and coronal CT reconstruction images. Mural thickness was defined as the greatest mural thickness perpendicular to the long axis of the colon depicted in the plane in which CRC was best visualized. In each case, a circular or elliptical ROI of > 50 mm^2 was placed on the slice section with the largest tumor portion (Fig. 2). The ROI was measured three times in the brightest tumor area and measurements were averaged to minimize measurement errors (18).

Tumor-related variables were classified as follows: 1) tumor length: < 30 mm, 30 mm to < 60 mm, or ≥ 60 mm, 2) mural thickness: < 15 mm, and 3) enhancement: < 90 HU. Previous studies have considered that a tumor length of > 3 cm indicates high risk rectal cancer. In another study, it was reported that a tumor length of ≥ 6 cm was associated with a significantly higher risk of tumor recurrence and tumor-related death (19-21). However, there was no reference about mural thickness and enhancement in the previous studies. In the present study, the cut-off values used were the median values of continuous variables.

Tumor shape was classified as intraluminal polypoid, ulcerofungating/ulceroinfiltrative, or bulky pattern. An intraluminal polypoid mass was defined as an intraluminal protruding mass with a smooth margin, sharply delineated from the regional normal colorectal wall. An ulcerofungating or ulceroinfiltrative mass was defined as tumoral wall thickening with a height-to-width ratio of < 1. A bulky pattern was defined as 1) a tumor outer diameter larger than normal diameter and 2) an exophytic tumor component projecting > 1 cm beyond the presumed position of

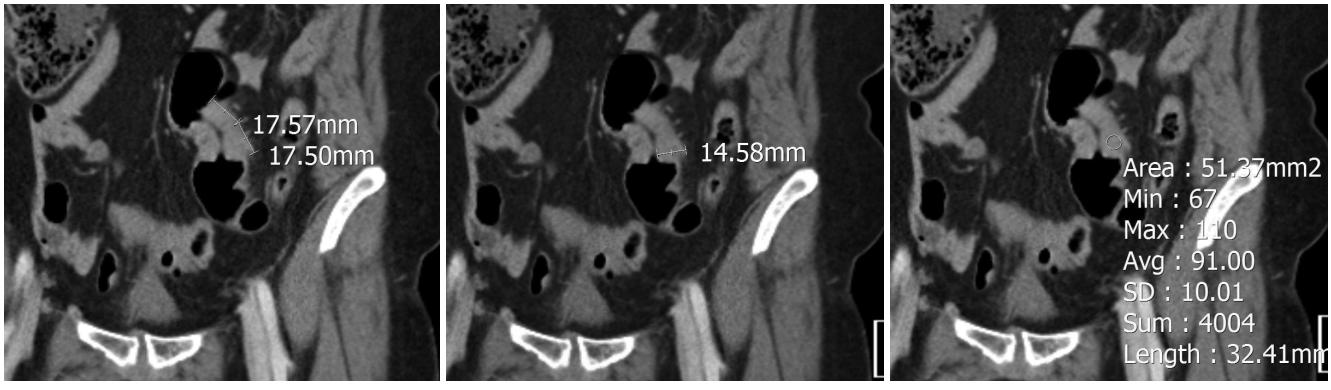

Fig. 2. Proximal sigmoid colon cancer in a 58-year-old woman. **(A)** Longitudinal tumor diameter, **(B)** tumor mural thickness, and **(C)** tumor enhancement (region of interest) of the primary cancer were measured.

the outermost tumoral wall (22, 23).

Pericolic fat infiltration was classified based on the absence of infiltration and presence of hazy, linear, or nodular infiltration. A normal peritumoral mesentery was considered not to exhibit pericolic fat infiltration. Hazy infiltration was classified as ill-defined or exhibiting slightly increased density in the peritumoral mesentery. Linear infiltration was defined as well-defined, increased density with a linear configuration in the peritumoral mesentery. Nodular infiltration was considered as a well-defined, nodular configured hyperdensity in the peritumoral mesentery (23).

Patient demographic characteristics including age, sex, tumor location, tumor cell type, serum carcinoembryonic antigen (CEA) level, and stage as defined by the American Joint Committee on Cancer and the International Union Against Cancer tumor, node, metastasis, seventh edition were recorded (24).

Reference Standard

Liver metastases were retrospectively reviewed by the two radiologists (S.J.C and C.R.S). On CT images, liver metastasis was defined as rim enhancement with central low attenuation. On Gd-EOB-DTPA enhanced MRI, liver metastasis was defined as rim enhancement and hyperintensity on T2-weighted image and diffusion weighted imaging with a defect in the hepatobiliary phase. On positron emission tomography-computed tomography (PET-CT), liver metastasis exhibited hypermetabolism (25-27). The presence of liver metastasis in our cohort was determined by operation (n = 11), percutaneous biopsy (n = 5), or imaging studies (n = 40). For establishing the diagnosis of liver metastases based on imaging findings, it was necessary that at least one of the following conditions was satisfied: (a) lesions showed an interval size reduction after chemotherapy (n = 21); (b) lesions showed interval size progression (n = 9); (c) lesions showed hypermetabolism on 18F-fluorodeoxyglucose PET-CT (n = 22). Twelve patients with liver metastases were diagnosed by CT and PET/CT (size progression, n = 10; size reduction, n = 2). We reviewed the indeterminate hepatic lesions on CT or MRI and determined an equivocal case (per patient) by consensus. An equivocal case was defined as the one in which the two readers could not determine whether the patient had liver metastases or not. Synchronous liver metastases were defined as liver metastases detected by preoperative CT or MRI or during primary tumor resection (28).

Statistical Analysis

Categorical data are presented as percentages, frequencies, and differences between proportions, and they were compared using the chi-squared test or Fisher's exact test, as appropriate. Continuous data with a significantly skewed distribution are expressed as medians, and they were compared using the Mann-Whitney U-test. Mean values of continuous variables with normal distributions were compared using the unpaired Student's t-test. Univariate analysis and multivariate logistic regression analysis with entry analysis were used to identify risk factors independently and significantly associated with the presence of synchronous metastases. Variables with a p-value of < 0.05 on univariate analysis were included in final multivariate models. receiver operating characteristic (ROC) curve analysis results for factors that were identified by logistic regression analysis. The analysis was performed using SPSS/PC version 20.0 (IBM Corp., Armonk, NY, USA) and Medcalc software (Medcalc for Windows, version 16.4.3; MedCalc Software bvba, Ostend, Belgium), and p-values of < 0.05 were considered statistically significant.

RESULTS

Patient Demographics

The demographics of patients with CRC and liver mass are shown in Tables 1, 2. Of the 197 patients, 56 (28.4%) had detectable synchronous liver metastases; 31 (55%) had metastasis confined to the liver and 25 (45%) had metastasis to another organ.

Thirty-one (31/56, 55%) patients underwent CT only and 25 (25/56, 45%) patients underwent both CT and MRI. Among the patients who underwent CT alone, only one patient was an equivocal case. This equivocal lesion was not detected in the initial CT interpretation in real clinical practice and additional MRI was not performed. In the present study, this lesion was not detected by either reader during retrospective CT evaluation. However, this lesion had increased in size on the follow-up CT scan after 9 months and it was confirmed to be metastasis (Fig. 3). Among the patients who underwent both CT and MRI, 12 patients (12/25, 48%) had 15 equivocal hepatic lesions detected by CT. One of these 15 lesions (1/15, 7%) was identified as liver me-

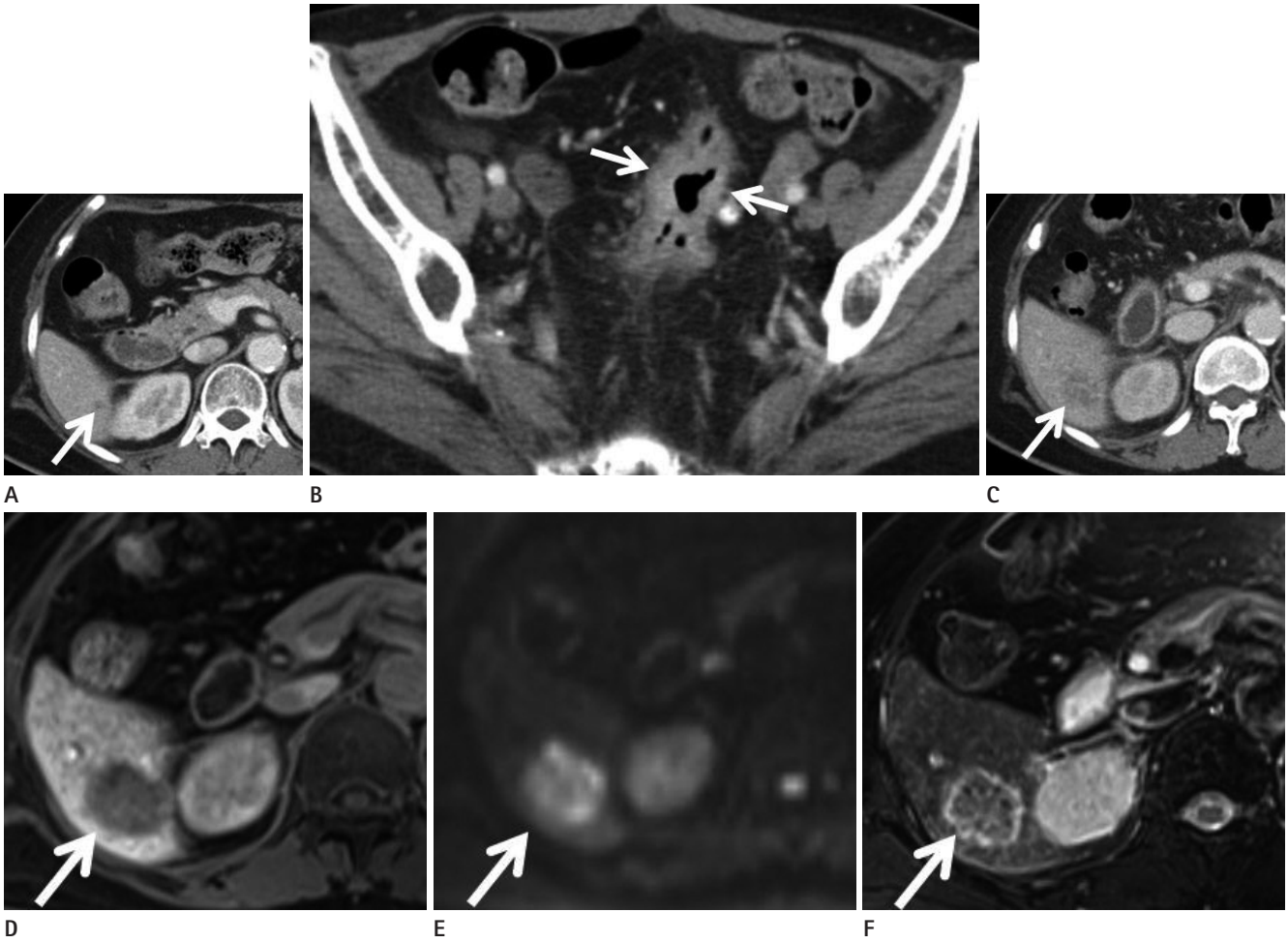

Fig. 3. Liver metastasis from recto-sigmoid colon cancer in a 67-year-old woman. **(A)** Transverse CT image shows a tiny indeterminate hypoattenuating lesion (arrow) in hepatic segment VI. **(B)** Transverse CT image shows a primary tumor (arrows). Tumor enhancement was 126 HU, suggestive of high risk. **(C)** The tiny lesion had increased in size as determined by follow-up CT 9 months later (arrow). **(D)** Gadoxetic acid-enhanced hepatobiliary phase image shows a hypointense lesion (arrow) in hepatic segment VI. **(E)** Diffusion weighted images (b = 1000 sec/mm^2) and **(F)** T2-weighted images demonstrate a hyperintense lesion (arrows). This lesion was considered to be metastasis based on analyses of serial CT and magnetic resonance images.
CT = computed tomography

tastasis on MRI, and the other 14 lesions were interpreted as benign hepatic lesions. Three patients had small liver metastases which were detected by MRI but not by CT (Fig. 4). However, among them, there were no equivocal cases because they had other definite liver metastases.

Results of Image Analysis

The CT findings of primary tumors are summarized in Table 3. Longitudinal diameter, mural thickness, and enhancement were significant higher in patients with liver metastases than in patients without liver metastases ($p < 0.05$). With respect to lesion shape, 23% (13/56) of patients with liver metastases exhibited a bulky pattern, whereas 23% (33/141) of patients without liver metastases had intraluminal polypoid lesions ($p < 0.001$). With respect to pericolic fat infiltration, 77% (43/56) of patients with liver metastases exhibited nodular or linear infiltration, whereas 49% (69/141) of patients without liver metastases exhibited hazy infiltration or absence of infiltration. Fourteen (25%, 14/56) patients with liver metastases had pulmonary metastases, whereas only one patient (0.7%, 1/141) without liver metastases had pulmonary metastases ($p < 0.001$).

Univariate and Multivariate Analyses

Univariate analysis showed that the risk factors associated with liver metastases were as follows: T stage ($p = 0.005$), N stage ($p = 0.031$ and $p < 0.001$), tumor diameter ($p = 0.021$ and $p = 0.001$),

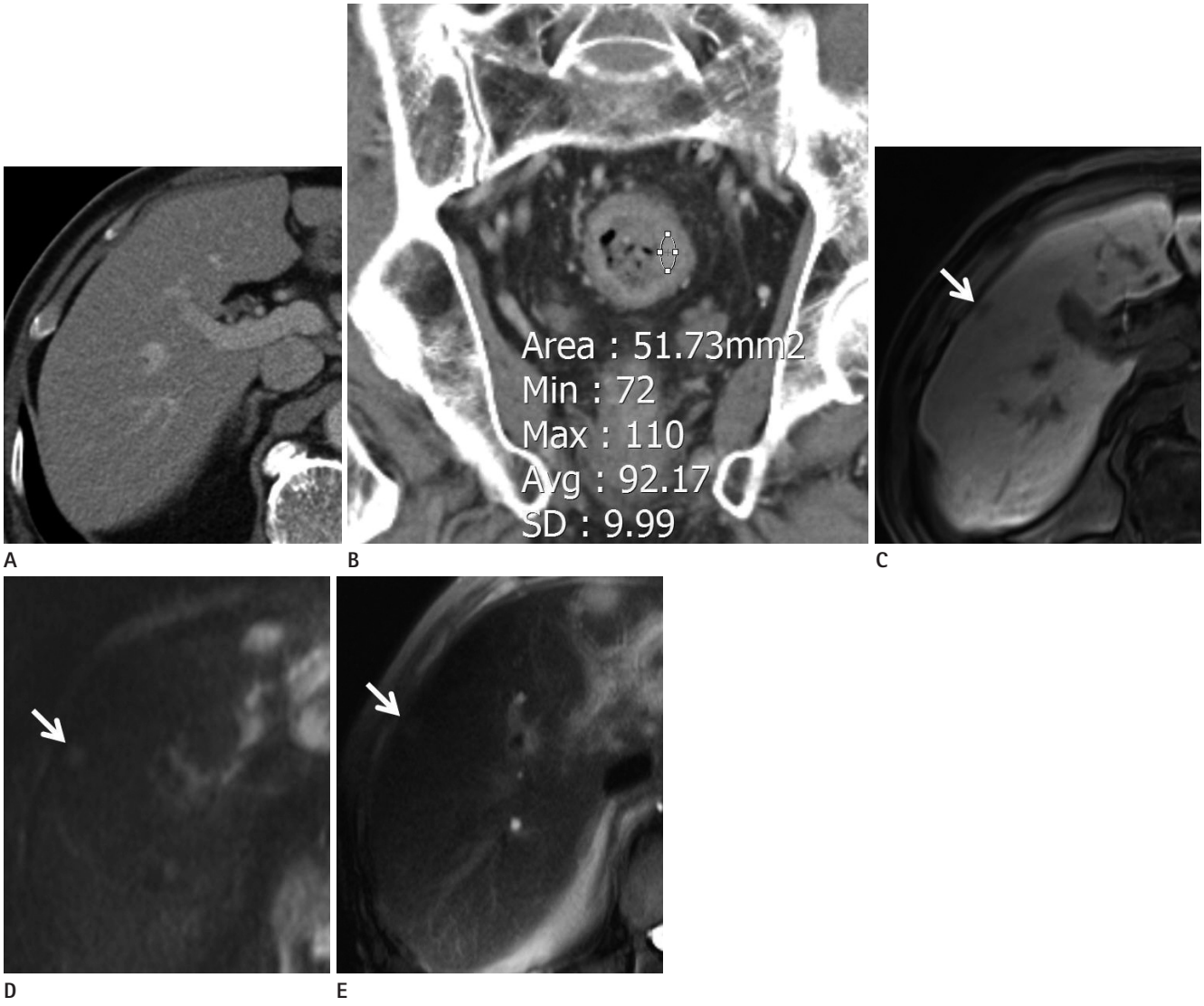

Fig. 4. Liver metastasis from recto-sigmoid colon cancer in an 80-year-old man. **(A)** Transverse CT did not depict a definite abnormal lesion in hepatic segment V. **(B)** Coronal reconstruction image shows a primary tumor. Its enhancement was 92 Hounsfield units, suggestive of high risk. Magnetic resonance images were obtained 3 days after initial CT. **(C)** Gadoxetic acid-enhanced hepatobiliary phase image shows a hypointense lesion (arrow) in hepatic segment V. **(D)** Diffusion weighted images (b = 800 sec/mm^2) and **(E)** T2-weighted images demonstrate a hyperintense lesion (arrows). This lesion was confirmed to be metastasis by tumorectomy.
CT = computed tomography

mural thickness ($p < 0.001$), tumor enhancement ($p < 0.001$), CEA level ($p < 0.001$), and pulmonary metastases ($p < 0.001$) (Table 4). Multivariate analysis identified the following risk factors: tumoral enhancement ($p = 0.048$), pulmonary metastases ($p = 0.014$), N stage ($p < 0.001$), and serum CEA level ($p = 0.027$) (Table 5).

Diagnostic Performance

Lymph node metastases showed the largest area under the ROC curve (0.818, $p < 0.001$) (Fig. 5, Table 6). Also, lymph node metastases showed a statistically significant difference between other factors except CEA; vs. T staging, $p = 0.001$; vs. diameter, $p = 0.005$; vs. mural thickness, $p = 0.001$; vs. enhancement, $p = 0.012$; vs. pulmonary metastases, $p < 0.001$; vs. CEA, $p = 0.11$.

DISCUSSION

This study demonstrated that primary CRC enhancement, the presence of pulmonary metastasis, N2 stage, and CEA level significantly predicted the presence of synchronous liver metas-

tases. Our results suggest that radiologists should be more concerned about small hepatic lesions and should not hesitate to request MRI or percutaneous needle biopsy when equivocal hepatic lesions are encountered, and that surgeons should concentrate on small hepatic lesions during laparotomy in CRC patients with high risk factors. Furthermore, we recommend that retrospective reviews should be conducted for missed hepatic lesions and follow-ups should be conducted more frequently in such patients.

Primary tumor enhancement has not been well evaluated, and the results of the present study suggested the possibility of a correlation between higher tumor enhancement and liver metastases. However, previous studies have reported contrary results. In one study, the researchers showed that among CT perfusion parameters, the mean blood flow, which reflects the flow rate through the vasculature, was found to be related to tumor

Table 2. Characteristics of Liver Metastases

Variable	No. of Patients (*n* = 56)
No. of liver metastases	
< 5	31
≥ 5	25
Size of liver metastases	
< 5 cm	28
≥ 5 cm	28
Involvement of hepatic lobes	
One lobe	23
Two lobes	33
Diagnosis of metastases	
Percutaneous biopsy	5
Surgical tumorectomy	11
Imaging study	40
Size reduction after chemotherapy	21
Size progression	9
Positive on PET/CT	22

Table 1. Clinico-Pathological and Radiological Data of Colorectal Cancer Patients with or without Hepatic Metastases

Variable	Patients with Liver Metastasis (*n* = 56)	Patients without Liver Metastasis (*n* = 141)	*p*-Value
Age	66 ± 12.4	64 ± 12.8	
Sex (M:F)	33:23	89:52	
Tumor location, n (%)			
Right colon	9 (16)	32 (22.8)	
Left colon	7 (12.5)	24 (16.7)	
Rectosigmoid junction	21 (37.5)	44 (31.3)	
Rectal ampulla	19 (34)	39 (27.8)	
Synchronous	0	2 (1.4)	
Cell type, n (%)			
Adenocarcinoma			
Well differentiated	3 (5.4)	12 (8.5)	
Moderate	45 (80)	115 (81.6)	
Poorly	2 (3.6)	3 (2.1)	
Mucinous adenocarcinoma	5 (9.2)	8 (5.7)	
Signet ring cell carcinoma	1 (1.8)	3 (2.1)	
pT staging			
T1	0	6 (5)	
T2	0	24 (20)	
T3	24 (69)	83 (69)	
T4	11 (31)	7 (6)	
pN staging			
N0	5 (14)	81 (94.5)	
N1	11 (31)	36 (3)	
N2	19 (55)	3 (2.5)	
Unresectable condition, n (%)	14 (25%, 14/56)	8 (6%, 8/131)	
Neoadjuvant CRT, n (%)	7 (13%, 7/56)	13 (10%, 13/131)	
CEA (μg/L)*	177.8 ± 593.3	10.4 ± 31.0	0.001

*Means and standard deviations are reported in parentheses.
CEA = carcinoembryonic antigen, CRT = chemoradiotherapy

Table 3. Radiological Finding of Primary Colorectal Cancer with or without Liver Metastases

Variable	Patients with Liver Metastasis (*n* = 56)	Patients without Liver Metastasis (*n* = 141)	*p*-Value
Longitudinal diameter (mm)*	54.9 ± 18.9	42.3 ± 19.5	< 0.001
Mural thickness (mm)*	18.4 ± 8.8	14.4 ± 6.0	0.003
Enhancement (ROI, HU)*	91.4 ± 10.3	83.9 ± 11.1	< 0.001
Shape of tumor, n (%)			< 0.001
Intraluminal polypoid	0 (0)	33 (23)	
Ulcerofungating or Ulceroinfiltrative pattern	40 (71)	102 (72)	
Bulky pattern	16 (29)	6 (5)	
Pericolic fat infiltration, n (%)			< 0.001
None	0 (0)	33 (23)	
Hazy infiltration	13 (23)	36 (26)	
Linear infiltration	29 (52)	59 (42)	
Nodular infiltration	14 (25)	13 (9)	
Pulmonary metastases, n (%)	14 (25)	1 (0.7)	< 0.001

*Means and standard deviations are reported in parentheses.
HU = Hounsfield units, ROI = region of interest

Table 4. Risk Factors of Liver Metastases as Determined by Univariate Analysis

Variable	OR	95% CI	*p*-Value
Age	1.005	0.981, 1.030	0.664
Sex	0.779	0.415, 1.463	0.437
T staging (vs. T1 and T2)			
T3 and T4	18.160	2.423, 136.117	0.005
N staging (vs. N0)			
N1	3.068	1.109, 8.491	0.031
N2	26.185	10.020, 68.426	< 0.001
Location of primary tumor	1.970	0.963, 4.030	0.063
Diameter of primary tumor (vs. < 30 mm)			
30 ≤ x < 60	3.726	1.218, 11.396	0.021
60 ≤	6.648	2.079, 21.260	0.001
Mural thickness (vs. < 15 mm)			
15 ≤ x	3.799	1.925, 7.495	< 0.001
Enhancement (ROI) of tumor (vs. < 90 HU)			
90 ≤ x	1.054	1.033–1.098	< 0.001
Cell type	1.060	0.458–2.453	0.891
CEA	1.015	1.007–1.023	< 0.001
Pulmonary metastases	46.667	5.961–365.359	< 0.001

CEA = carcinoembryonic antigen, CI = confidence interval, OR = odds ratio, ROI = region of interest

Table 5. Risk Factors of Liver Metastases as Determined by Multivariate Analysis

Variable	OR	95% CI	*p*-Value
T staging (vs. T1 and T2)			
T3 and T4	4.453	0.492, 40.322	0.184
N staging (vs. N0)			
N1	1.698	0.533, 5.406	0.370
N2	9.186	3.018, 27.956	< 0.001
Diameter of primary tumor (vs. < 30 mm)			
30 ≤ x < 60	1.948	0.523, 7.250	0.320
60 ≤	2.085	0.504, 8.621	0.310
Mural thickness (vs. < 1 5 mm)			
15 ≤ x	1.260	0.509, 3.123	0.617
Enhancement (ROI) of tumor (vs. < 90 HU)			
90 ≤ x	2.450	1.009, 5.953	0.048
CEA	1.013	1.002, 1.026	0.027
Pulmonary metastases	17.855	1.790, 178.100	0.014

CEA = carcinoembryonic antigen, CI = confidence interval, OR = odds ratio, ROI = region of interest

vascularity, and it was found to be lower in poorly differentiated tumors than in well differentiated or moderately differentiated tumors (18). Another study concluded that poorly perfused tumors have poorer outcomes (29). These discrepancies may have been caused by the ROI measurement method used in the present study, as we located ROIs in the area of greatest enhancement, which cannot accurately reflect intratumoral heterogeneity. When we examined the correlation between attenuation and cell type, no relation was found. We supposed that the number of patients with mucinous adenocarcinoma was too small to obtain appropriate statistical power.

The strong relation between pulmonary metastases and liver metastases can be explained by the cascade hypothesis. The liver is the first major organ encountered by venous blood draining from the gastrointestinal tract. Therefore, cancer cells traveling by the hematogenous spread are likely to arrive within the sinusoids of the liver (30). According to the cascade hypothesis, metastasis in the first organ encountered may act as the centrum for dissemination of tumor cells to other organs (e.g., lungs),

and in turn, lung metastasis may then act as the centrum for further dissemination (31). This hypothesis is supported by necropsy data of adenocarcinoma of the upper rectum and that of other carcinomas in the digestive system (31, 32).

We found that N2 stage disease presents a higher risk of liver metastases than N0 stage disease. A prospective, large population-based study showed that lymph node metastasis was an independent risk factor of synchronous liver metastases in CRC (33). However, recent studies have shown that radiologic lymph node metastases from rectal MRI did not significantly predict liver metastases (16, 34). Further studies are evidently needed for assessing radiologic lymph node metastases in CRC.

Use of chemotherapy and the proportion of patients who undergo hepatic surgery continue to increase and these factors have significantly increased the survival rates (8). Furthermore, retrospective studies conducted in patients who have undergone complete surgical resection of liver metastasis have suggested that resection improves the overall survival rates. Thus, early and accurate detection of liver metastases is clinically important because it can significantly affect the choice of therapeutic approach and prognosis. However, little is known regarding the prevalence of synchronous liver metastases in CRC and few epidemiologic studies have addressed the overall metastasis rate in CRC. There is some concern that multiple detector computed tomography (MDCT) images may not accurately characterize small hepatic nodules or sufficiently differentiate small liver metastases and small hepatic cysts or hemangiomas (35-37). Furthermore, MDCT is less able to detect liver metastases than MRI when an extracellular contrast agent is used (38, 39).

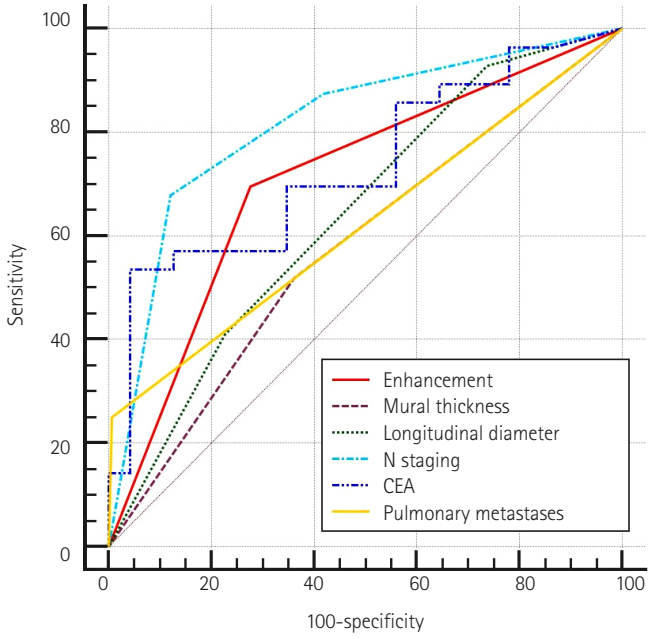

Fig. 5. Receiver operating characteristic curve analysis results for factors that were found to be positively associated with the presence of liver metastasis by logistic regression analysis.
CEA = carcinoembryonic antigen

Recently, a multicenter clinical trial was initiated to validate the use of DW-MRI for screening of synchronous liver metastases in CRC. The aim of this trial was to determine how well DW-MRI identifies liver metastases as compared with routine CT (32). We suggest that screening DW-MRI should be used in patients with risk factors of liver metastases detected by baseline CT.

Our study has several limitations, such as a retrospective design and the use of a combination of pathologic and follow-up imaging findings. Furthermore, the presence of multiple metastases and the diminutive size of many nodules frequently resulted in unnecessary or impractical biopsies of individual lesions. In addition, as we have mentioned above, ROI-based assessment cannot adequately reflect intratumoral heterogeneity, and the selection of ROI locations introduces a possible bias. We suggest that further studies should be conducted to refine the

Table 6. ROC Curve Analysis Results for Factors Identified by Logistic Regression Analysis

Variable	Sensitivity (%)	Specificity (%)	AUC	95% CI	*p*-Value
T staging	41	85	0.696	0.627, 0.760	< 0.001
N staging	68	88	0.818	0.756, 0.869	< 0.001
Longitudinal diameter	93	26	0.688	0.618, 0.752	< 0.001
Mural thickness	73	58	0.657	0.586, 0.723	< 0.001
Enhancement (ROI)	66	72	0.710	0.641, 0.772	< 0.001
CEA	54	96	0.733	0.666, 0.794	< 0.001
Pulmonary metastases	25	99	0.621	0.550, 0.689	< 0.001

AUC = area under the ROC curve, CEA = carcinoembryonic antigen, CI = confidence interval, OR = odds ratio, ROC = receiver operating characteristic, ROI = region of interest

measurements of whole tumor volume enhancement.

In conclusion, our findings suggest that tumor enhancement and the presence of pulmonary metastases as determined by MDCT could be used to predict the risk of development of synchronous liver metastases in CRC patients. We suggest that equivocal hepatic lesions should be assessed thoroughly for metastases in patients with high risk factors.

REFERENCES

1. Jemal A, Bray F, Center MM, Ferlay J, Ward E, Forman D. Global cancer statistics. *CA Cancer J Clin* 2011;61:69-90
2. Ferlay J, Shin HR, Bray F, Forman D, Mathers C, Parkin DM. Estimates of worldwide burden of cancer in 2008: GLOBOCAN 2008. *Int J Cancer* 2010;127:2893-2917
3. Mella J, Biffin A, Radcliffe AG, Stamatakis JD, Steele RJ. Population-based audit of colorectal cancer management in two UK health regions. Colorectal Cancer Working Group, Royal College of Surgeons of England Clinical Epidemiology and Audit Unit. *Br J Surg* 1997;84:1731-1736
4. Paschos KA, Bird N. Current diagnostic and therapeutic approaches for colorectal cancer liver metastasis. *Hippokratia* 2008;12:132-138
5. Geoghegan JG, Scheele J. Treatment of colorectal liver metastases. *Br J Surg* 1999;86:158-169
6. Welch JP, Donaldson GA. The clinical correlation of an autopsy study of recurrent colorectal cancer. *Ann Surg* 1979;189:496-502
7. Schmiegel W, Pox C, Reinacher-Schick A, Adler G, Arnold D, Fleig W, et al. S3 guidelines for colorectal carcinoma: results of an evidence-based consensus conference on February 6/7, 2004 and June 8/9, 2007 (for the topics IV, VI and VII). *Z Gastroenterol* 2010;48:65-136
8. Kopetz S, Chang GJ, Overman MJ, Eng C, Sargent DJ, Larson DW, et al. Improved survival in metastatic colorectal cancer is associated with adoption of hepatic resection and improved chemotherapy. *J Clin Oncol* 2009;27:3677-3683
9. Minami Y, Kudo M. Radiofrequency ablation of liver metastases from colorectal cancer: a literature review. *Gut Liver* 2013;7:1-6
10. Tomlinson JS, Jarnagin WR, DeMatteo RP, Fong Y, Kornprat P, Gonen M, et al. Actual 10-year survival after resection of colorectal liver metastases defines cure. *J Clin Oncol* 2007;25:4575-4580
11. Abdalla EK, Adam R, Bilchik AJ, Jaeck D, Vauthey JN, Mahvi D. Improving resectability of hepatic colorectal metastases: expert consensus statement. *Ann Surg Oncol* 2006;13:1271-1280
12. Rees M, Tekkis PP, Welsh FK, O'Rourke T, John TG. Evaluation of long-term survival after hepatic resection for metastatic colorectal cancer: a multifactorial model of 929 patients. *Ann Surg* 2008;247:125-135
13. Ye LC, Liu TS, Ren L, Wei Y, Zhu DX, Zai SY, et al. Randomized controlled trial of cetuximab plus chemotherapy for patients with KRAS wild-type unresectable colorectal liver-limited metastases. *J Clin Oncol* 2013;31:1931-1938
14. Cremolini C, Loupakis F, Antoniotti C, Lupi C, Sensi E, Lonardi S, et al. FOLFOXIRI plus bevacizumab versus FOLFIRI plus bevacizumab as first-line treatment of patients with metastatic colorectal cancer: updated overall survival and molecular subgroup analyses of the open-label, phase 3 TRIBE study. *Lancet Oncol* 2015;16:1306-1315
15. Hunter CJ, Garant A, Vuong T, Artho G, Lisbona R, Tekkis P, et al. Adverse features on rectal MRI identify a high-risk group that may benefit from more intensive preoperative staging and treatment. *Ann Surg Oncol* 2012;19:1199-1205
16. Kim YC, Kim JK, Kim MJ, Lee JH, Kim YB, Shin SJ. Feasibility of mesorectal vascular invasion in predicting early distant metastasis in patients with stage T3 rectal cancer based on rectal MRI. *Eur Radiol* 2016;26:297-305
17. Screening for synchronous metastases in colorectal cancer with DW-MRI (SERENADE). Available at: https://clinicaltrials.gov/ct2/show/NCT02246634. Published Sep 5, 2014. Accessed Apr 12, 2017
18. Kim JW, Jeong YY, Chang NK, Heo SH, Shin SS, Lee JH, et al. Perfusion CT in colorectal cancer: comparison of perfusion parameters with tumor grade and microvessel density. *Korean J Radiol* 2012;13 Suppl 1:S89-S97
19. Russell AH, Harris J, Rosenberg PJ, Sause WT, Fisher BJ, Hoffman JP, et al. Anal sphincter conservation for patients with adenocarcinoma of the distal rectum: long-term results of radiation therapy oncology group protocol 89-02. *Int J Radiat Oncol Biol Phys* 2000;46:313-322
20. Mohiuddin M, Marks G, Bannon J. High-dose preoperative

radiation and full thickness local excision: a new option for selected T3 distal rectal cancers. *Int J Radiat Oncol Biol Phys* 1994;30:845-849
21. Gertler R, Rosenberg R, Schuster T, Friess H. Defining a high-risk subgroup with colon cancer stages I and II for possible adjuvant therapy. *Eur J Cancer* 2009;45:2992-2999
22. Horton KM, Abrams RA, Fishman EK. Spiral CT of colon cancer: imaging features and role in management. *Radiographics* 2000;20:419-430
23. Kim JE, Lee JM, Baek JH, Moon SK, Kim SH, Han JK, et al. Differentiation of poorly differentiated colorectal adenocarcinomas from well- or moderately differentiated colorectal adenocarcinomas at contrast-enhanced multidetector CT. *Abdom Imaging* 2015;40:1-10
24. Filippone A, Ambrosini R, Fuschi M, Marinelli T, Genovesi D, Bonomo L. Preoperative T and N staging of colorectal cancer: accuracy of contrast-enhanced multi-detector row CT colonography--initial experience. *Radiology* 2004;231:83-90
25. Sica GT, Ji H, Ros PR. CT and MR imaging of hepatic metastases. *AJR Am J Roentgenol* 2000;174:691-698
26. Chung WS, Kim MJ, Chung YE, Kim YE, Park MS, Choi JY, et al. Comparison of gadoxetic acid-enhanced dynamic imaging and diffusion-weighted imaging for the preoperative evaluation of colorectal liver metastases. *J Magn Reson Imaging* 2011;34:345-353
27. Seo HJ, Kim MJ, Lee JD, Chung WS, Kim YE. Gadoxetate disodium-enhanced magnetic resonance imaging versus contrast-enhanced 18F-fluorodeoxyglucose positron emission tomography/computed tomography for the detection of colorectal liver metastases. *Invest Radiol* 2011;46:548-555
28. Adam R, de Gramont A, Figueras J, Kokudo N, Kunstlinger F, Loyer E, et al. Managing synchronous liver metastases from colorectal cancer: a multidisciplinary international consensus. *Cancer Treat Rev* 2015;41:729-741
29. Goh V, Glynne-Jones R. Perfusion CT imaging of colorectal cancer. *Br J Radiol* 2014;87:20130811
30. Weiss L, Grundmann E, Torhorst J, Hartveit F, Moberg I, Eder M, et al. Haematogenous metastatic patterns in colonic carcinoma: an analysis of 1541 necropsies. *J Pathol* 1986; 150:195-203
31. Viadana E, Bross ID, Pickren JW. The metastatic spread of cancers of the digestive system in man. *Oncology* 1978;35: 114-126
32. Weiss L, Voit A, Lane WW. Metastatic patterns in patients with carcinomas of the lower esophagus and upper rectum. *Invasion Metastasis* 1984;4:47-60
33. Mantke R, Schmidt U, Wolff S, Kube R, Lippert H. Incidence of synchronous liver metastases in patients with colorectal cancer in relationship to clinico-pathologic characteristics. Results of a German prospective multicentre observational study. *Eur J Surg Oncol* 2012;38:259-265
34. Kang KA, Jang KM, Kim SH, Kang TW, Cha DI. Risk factor assessment to predict the likelihood of a diagnosis of metastasis for indeterminate hepatic lesions found at computed tomography in patients with rectal cancer. *Clin Radiol* 2017; 72:473-481
35. Jones EC, Chezmar JL, Nelson RC, Bernardino ME. The frequency and significance of small (less than or equal to 15 mm) hepatic lesions detected by CT. *AJR Am J Roentgenol* 1992;158:535-539
36. Krakora GA, Coakley FV, Williams G, Yeh BM, Breiman RS, Qayyum A. Small hypoattenuating hepatic lesions at contrast-enhanced CT: prognostic importance in patients with breast cancer. *Radiology* 2004;233:667-673
37. Goshima S, Kanematsu M, Watanabe H, Kondo H, Shiratori Y, Onozuka M, et al. Hepatic hemangioma and metastasis: differentiation with gadoxetate disodium-enhanced 3-T MRI. *AJR Am J Roentgenol* 2010;195:941-946
38. Kim YK, Park G, Kim CS, Yu HC, Han YM. Diagnostic efficacy of gadoxetic acid-enhanced MRI for the detection and characterisation of liver metastases: comparison with multidetector-row CT. *Br J Radiol* 2012;85:539-547
39. Böttcher J, Hansch A, Pfeil A, Schmidt P, Malich A, Schneeweiss A, et al. Detection and classification of different liver lesions: comparison of Gd-EOB-DTPA-enhanced MRI versus multiphasic spiral CT in a clinical single centre investigation. *Eur J Radiol* 2013;82:1860-1869

다중검출 전산화단층촬영을 이용한 대장암 간전이의 위험인자 연구

서초롱 · 최승준* · 김형식

목적: 다중검출 전산화단층촬영 영상을 이용하여 대장암의 간전이를 예측할 수 있는 위험인자를 알아보고자 하였다.
대상과 방법: 197명의 다중검출 전산화단층촬영 영상에서 원발 종괴가 보인 대장암 환자를 대상으로 영상을 분석하였다. 저자들은 원발 종괴의 길이, 벽두께, 음영을 측정하고 다른 전이 여부를 평가하였다. 일변량 분석과 다변량 로지스틱 회귀분석법을 이용하여 간전이의 위험인자를 확인하였다.
결과: 197명의 대장암 환자 중 간전이가 있는 환자는 56명이었다. 종괴의 조영증강이 90 Hounsfield units 이상인 경우, 그 이하인 경우보다 간전이 위험도가 증가하였다[odds ratio (OR): 2.619, p = 0.034]. 폐전이가 있는 환자의 경우에도 없는 환자보다 간전이의 위험도가 증가하였다(OR: 14.218, p = 0.025). 림프절 전이(N2 vs. N0)와 carcinoembryonic antigen (CEA) 수치도 간전이를 예측하는 독립 인자로 확인되었다(OR: 8.766, p < 0.001; OR: 1.012, p = 0.048).
결론: 대장암의 간전이는 원발 종괴의 조영증강 정도, 폐전이의 유무, 림프절 전이 및 CEA 수치와 관련이 있다.

가천대학교 길병원 영상의학과